ACS APPLIED MATERIALS & INTERFACES

Research Article

www.acsami.org

Rapid and Quantitative Detection of Prostate Specific Antigen with a Quantum Dot Nanobeads-Based Immunochromatography Test Strip

Xue Li,[†] Wenbin Li,[§] Qiuhua Yang,[†] Xiaoqun Gong,[‡] Weisheng Guo,[†] Chunhong Dong,[†] Junqing Liu,[†] Lixue Xuan,*[,§] and Jin Chang*[,†]

[†]Institute of Nanobiotechnology, School of Materials Science and Engineering, School of Precision Instruments and Opto-Engineering, Tianjin University and Tianjin Key Laboratory of Composites and Functional Materials, Tianjin 300072, P.R. China

[‡]School of Life Science, Tianjin University, Tianjin 300072, P.R. China

[§]Cancer Hospital, Chinese Academy of Medical Sciences & Peking Union Medical College, Beijing, 100021, P.R. China

Supporting Information

ABSTRACT: Convenient and fast testing using an immunochromatography test strip (ICTS) enables rapid yes/no decisions regarding a disease to be made. However, the fundamental limitations of an ICTS, such as a lack of quantitative and sensitive analysis, severely hampers its application in reliable medical testing for the early detection of cancer. Herein, we overcame these limitations by integrating an ICTS with quantum dot nanobeads (QD nanobeads), which were fabricated by encapsulating QDs within modified poly(*tert*-butyl acrylate-*co*-ethyl acrylate-*co*-methacrylic acid) and served as a robust signal-generating reagent for the ICTS. Prostate specific antigen (PSA) was used as a model analyte to demonstrate the performance of the QD nanobeads-based ICTS platform. Under optimized conditions, the concentration of PSA could be determined within 15 min with high sensitivity and specificity using only 40 μL of sample. The detection limit was enhanced by ~12-fold compared with that of an ICTS that used QDs encapsulated by commercial 11-mercaptoundecanoic acid (QDs@MUA) as the signal-generating reagent. At the same time, the possible clinical utility of this approach was demonstrated by measurements recorded from PSA-positive patient specimens. Our data suggest that the QD nanobeads-based ICTS platform is not only rapid and low-cost but also highly sensitive and specific for use in quantitative point-of-care diagnostics; thus, it holds promise for becoming a part of routine medical testing for the early cancer of detection.

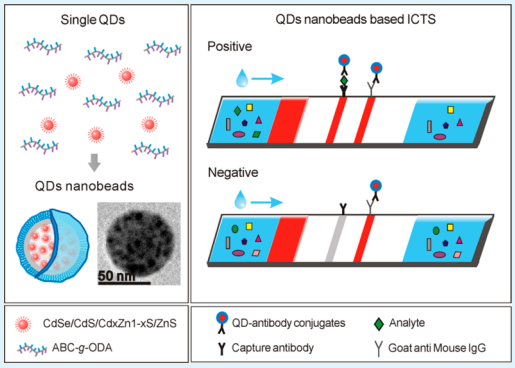

KEYWORDS: *quantum dot nanobeads, immunochromatography test strip, prostate specific antigen (PSA), quantitative detection, early cancer detection*

1. INDRODUCTION

The presence of certain cancer protein biomarkers or irregular protein concentrations can be a sign of disease-related biological processes.[1] Protein-sensing methods provide the potential to enable and hasten early disease detection and to rationalize treatments, especially for cancers.[1,2] The early diagnosis of cancer is very critical to improve the cure and survival rates.[3] However, identifying specific cancer protein biomarkers for early cancer detection remains a longstanding barrier for cancer therapy. During the past decade, although methodological advances have been achieved, detection methods are still severely restricted because they require expensive instruments, highly skilled personnel to perform the procedures, and tedious analysis time. Therefore, the demand for point-of-care diagnostic tests that can be carried out for on-the-spot patient care is enormous.

The immunochromatography test strip (ICTS) is the most common commercial point-of-care diagnostic format.[4] This device depends upon fluid migration or flow technology, which includes porous membranes, antibodies, and a visible signal-generating entity. It benefits from several advantages:[4,5] a short time is consumed for sample purification, no incubation and washing steps are required before analysis, small sample volumes are needed, and skilled technicians are not required. As a viable point-of-care diagnostic, the signal-generating reagent used in an ICTS plays a critical role for producing and transducing the signal in an immunoassay,[6,7] which directly determines the ability of the ICTS to be used for quantitative detection as well as the sensitivity of the assay. Therefore, developing a robust signal-generating reagent is extremely critical for the quantitative and sensitive ICTS-mediated detection of analytes.

Great efforts have been made toward developing the signal-generating reagent. For this purpose, different materials have

Received: December 17, 2013
Accepted: April 19, 2014
Published: April 24, 2014

dx.doi.org/10.1021/am5012782 | ACS Appl. Mater. Interfaces 2014, 6, 6406−6414

been introduced, such as colloidal gold nanoparticles,[8−10] colored latex particles,[11,12] up-converting phosphors,[13,14] magnetic nanoparticles,[15,16] and organic fluorophores.[17,18] Among these candidates, quantum dots (QDs) as nanoscaled fluorescent labels have attracted great interest in biological and medical detection in recent years because of their fascinating optical and electronic properties.[19,20] Their high level of brightness and extraordinary photostability enables ultrasensitive detection for biomedical applications,[21,22] which also provides new opportunities for their use in an ICTS.[23,24] Although QDs have great potential to overcome the limitations of an ICTS, their longstanding problems of chemical and colloidal instability in biological environments after the phase-transfer procedure[25−27] might preclude them from facilitating accurate quantitative analysis. To address these issues, we put forward an amphiphilic molecule self-assembly strategy to encapsulate the QDs into nanobeads in order to obtain both good chemical and colloidal stability. The combination of QD nanobeads and ICTS can be used to generate rapid and quantitative point-of-care analysis.

Here, we report the fabrication of a kind of QD nanobeads with extraordinary stability in the development of an ICTS platform for cancer protein biomarker detection. Prostate specific antigen (PSA), which has been recognized as a valuable biomarker for prostate cancer diagnosis, was used as the model analyte in our study. The properties of these QD nanobeads, such as their structure, morphology, size distribution, and stability, were fully evaluated and further compared with QDs coated with conventional 11-mercaptoundecanoic acid (QDs@MUA). As expected, a higher fluorescent response was observed with the QD nanobeads-based ICTS. Then, the performance of the QD nanobeads-based ICTS platform was comprehensively displayed by investigating the effective reaction time, sensitivity, and specificity as well as the capability for quantitative detection. Our data proved that the assay can be completed in a rather short amount of time, providing facile quantitative detection of trace amounts of analyte with high sensitivity and specificity. Thus, as a first-response point-of-care device, the QD nanobeads-based ICTS may be widely used for early cancer detection in hospitals, communities, and even homes.

2. MATERIALS AND METHODS

2.1. Materials and Chemicals. Cadmium oxide (CdO, 99.5%), selenium powder (Se, 99.99%), sulfur (S, 99.98%), zinc oxide (ZnO, 99.9%), poly(*tert*-butyl acrylate-*co*-ethyl acrylate-*co*-methacrylic acid) (ABC triblock copolymer), and 11-mercaptoundecanoic acid (MUA) were purchased from Sigma-Aldrich and used without further purification. 1-Ethyl-3-(3-dimethyllaminopropyl)-carbodiimide hydrochloride (EDC) and *N*-hydroxysuccinimide (NHS) were purchased from GL Biochem (Shanghai) Ltd. and used without further purification. Fetal bovine serum (FBS) and bovine serum albumin (BSA) were purchased from Beijing Dingguo Biotechnology Co., Ltd. (China) and used without further purification. Mouse monoclonal antibody, goat anti-mouse IgG, reaction membrane, sample pad, conjugate pad, and absorbent pad were supplied by Bioscience (Tianjin) Diagnostic Technology Co., Ltd. and used as provided.

2.2. Synthesis of the ODA-Modified ABC Triblock Copolymer. To prepare the ODA-modified ABC triblock copolymer, a typical procedure[28,29] was used. One gram of ABC triblock copolymer was mixed with 20 mL of DMSO in a 150 mL three-necked flask. After stirring for 24 h at 60 °C, the solution was cooled to room temperature. A freshly prepared anhydrous solution of 0.16 g of ODA, dissolved in 10 mL of DMSO, was added. The solution was stirring for 30 min at 60 °C. After the addition of an anhydrous solution of 0.354 g of NHS in 6 mL of DMSO, 0.354 g of EDC was slowly added over the course of 40 min under vigorous stirring. The solution was allowed to react for 16 h at room temperature under constant stirring. After the reaction was complete, the resulting oily liquid was precipitated and rinsed with water five times to remove excess EDC and other byproducts. Then, the mixture was successively dialyzed against alcohol and distilled water for about 2 days for further purification. The final solution was lyophilized at −40 °C and stored at room temperature.

2.3. Synthesis of CdSe/CdS/$Cd_xZn_{1-x}S$/ZnS Nanocrystals. The core/shell QDs, CdSe/CdS/$Cd_xZn_{1-x}S$/ZnS, were synthesized on the basis of a successive ion-layer adsorption and reaction (SILAR) method. First, CdSe nanocrystals were prepared by a typical synthetic procedure:[30] 0.0386 g of CdO, 4 mL of ODE, and 0.4 mL of OA were added to a three-necked flask and heated at 260 °C under argon until complete dissolution of CdO. After cooling to room temperature, 0.5 g of TOPO and 2.5 g of ODA were added into the flask. The solution was heated at 300 °C under argon flow. A second solution, containing 0.14 g of selenium and 2 mL of TOP, was injected into the cadmium precursor solution quickly. Then, 250 °C was set as the growth temperature. After 10 min, the heating was stopped, and about 20 mL of methanol was added at room temperature to precipitate the CdSe nanocrystals. The particles were isolated by at least three hexane/methanol extractions. After centrifugation, the CdSe nanocrystals were dispersed in hexane.

Next, for shell growth, a procedure reported previously was slightly modified.[30,31] The solution containing the CdSe nanocrystals was mixed with 5.0 g of ODE and 1.5 g of ODA in another three-necked flask, and the system was kept at 100 °C under argon flow for 15 min to remove the hexane and other undesired materials. Subsequently, the system was heated at 240 °C for shell growth. The amount of the injection solution for each monolayer was determined by calculating the number of surface atoms for a given size of nanocrystal, and the Cd precursor (0.4 M) solutions, Zn precursor (0.4 M) solutions, and sulfur precursor (0.4 M) solutions were previously prepared. The reaction products were redissolved in hexane after extracting with methanol at least three times.

2.4. Preparation of QD Nanobeads, QDs@MUA, and QD−Antibody Conjugates. To prepare QD nanobeads, 40 μL of core/shell QDs and 2 mg of ABC-*g*-ODA were mixed with 960 μL of dichlormethane to form a uniform organic phase. Then, 10 mL of deionized (DI) water was added into the organic phase. The mixture was emulsified with an ultrasonicator at 100 W for 10 min. Then, the organic phase of the mixture was removed by magnetically stirring for 2 h. After that, the QD nanobeads were purified by washing at least three times with DI water and were collected by centrifugation. Final products were redissolved in phosphate-buffered saline (PBS) buffer solution (0.01 M, pH 7.4). For the control group, a typical ligand-exchange procedure was used.[25] The QDs (40 μL) were dissolved in 3 mL of chloroform. Then, a PBS buffer solution (0.01 M, pH 7.4) containing 0.03 g of MUA was added into the mixture. After a 2 h reaction, the aqueous layer containing QDs@MUA was extracted. Excess MUA was removed by centrifugation at least three times.

The QD−antibody conjugates were prepared by using a previously described method.[24] Water-soluble QDs (QD nanobeads, QDs@MUA), mouse monoclonal antibody, and EDC were mixed in PBS buffer solution (0.01 M, pH 7.4) at a QDs/antibody/EDC molar ratio of 1:10:4000. After 2 h of reacting at room temperature, the final QD−antibody conjugates were purified by centrifugation and stored in PBS buffer solution (0.01 M, pH 7.4, 0.5% BSA) overnight at 4 °C.

2.5. Test Strip Preparation. The test strip consists of a sample pad, conjugate pad, reaction membrane, absorbent pad, and backing card. The sample pad was pretreated with blocking buffer (pH 8.0, containing 20 mM tris (hydroxymethyl) aminomethane-HCl (Tris-HCl), 0.1% (w/v) Tween-20, and 0.5% (w/v) PVP) and dried at 37 °C for 2 h. After being diluted 20-fold in a second blocking buffer (pH 7.4, containing 0.01 M PBS, 5% (w/v) BSA, 7% (w/v) sucrose, 2% (w/v) PEG4000, and 0.1% (w/v) Tween-20), QD−antibody conjugates were dispensed onto the conjugated pad and dried at 37 °C for 2 h. Using the dispenser (XYZ-3050 BioJet Quanti 3000), the

desired volume of mouse monoclonal PSA antibody solution (1 mg/mL) and goat anti-mouse IgG (1 mg/mL) was dispensed on the reaction membrane to form the test zone and control zone, respectively. After 2 h of drying at 37 °C, all of the parts mentioned above were assembled on a plastic adhesive backing card, which was cut into 4 mm strips and stored at room temperature.

2.6. Design of the Test Strip Reader and Fluorescence Assay Procedure. The test strip reader was portable and laboratory-built,[24] which consisted of several core parts: a 405 nm laser diode, an optic fiber spectrometer, a miniprinter, a tablet computer, and a stepper motor. QDs were excited by the 405 nm laser diode. The generated fluorescence signal was converted into an electrical signal by the optic fiber spectrometer. The moving of the test strip was controlled by the stepper motor. All analysis procedures were automatically conducted and monitored by the tablet computer.

The fluorescence assay procedure was as follows: 40 μL of the sample solution was dropped onto the sample pad and flowed through the reaction membrane under capillary action. After the completion of the immunoreaction, the strip (in a cassette) was inserted into the laboratory-built test strip reader to read the fluorescence intensity of the test zone and the control zone to quantify the abundance of the analytes in the sample.

2.7. Characterization. Photoluminescence (PL) spectra were measured by a Gangdong F-280 spectrophotometer. Transmission electron microscopy (TEM) images were taken on a JEOL 100CX transmission electron microscope with an acceleration voltage of 100 kV. Particle size was analyzed by dynamic light scattering (DLS). Surface charge was analyzed by a zeta potential analyzer (Brookhaven Instruments). ^{1}H NMR was recorded on a NMR spectrometer (INOVA 500 MHz).

3. RESULTS AND DISCUSSION

3.1. Synthesis and Characterization of the QD Nanobeads. Synthesis of the ODA-modified ABC triblock copolymer (ABC-*g*-ODA) is demonstrated in Figure S1A, Supporting Information. The original ABC triblock copolymer ($M_w \approx 100\,000$) consisted of a polymethacrylic acid segment, a polyethyl acrylate segment, and a polybutyl acrylate segment, with a weight distribution of 77% combined butyl ethyl acrylates and 23% methacrylic acid. In this study, 30% of the −COOH groups in the ABC triblock copolymer were modified by ODA (estimated from the feed ratio of ODA and −COOH groups). The ^{1}H NMR spectra (see Supporting Information) was used to characterize the structure of ABC-*g*-ODA. As shown in Figure S1B, new peaks appeared at δ 0.88 and 2.80, which were attributed to the methylene protons adjacent to −CO−NH− after the grafting of ODA on the side chain, and the integrals at δ 3.65 (representing the protons of −COOH groups) decreased after grafting with ODA; these data confirmed the successful reaction between ODA and the −COOH groups in the ABC triblock copolymer side chains. Additionally, by calculating the peak integrals at δ 3.65, the grafting degree of ODA was about 27.0%.

Figure 1A illustrates the formation of the QD nanobeads: ABC-*g*-ODA self-assemble into micelles under ultrasonication (because of the strong hydrophobic interactions between the TOPO and ODA segments), QDs cluster inside the hydrophobic core of the micelles, and the block copolymer shell on the surface of the QDs stabilizes the particles in the aqueous solution, resulting in uniform and monodisperse hydrophilic nanobeads that were obtained after oil evaporation. TEM, DLS, and zeta potential analysis of the QD nanobeads were conducted to fully characterize their structural and optical properties, and the results are shown in Figure 1. The well-defined crystal structure in the HRTEM images (Figure 1B) revealed the high crystallinity of CdSe/CdS/$Cd_xZn_{1-x}S$/ZnS.

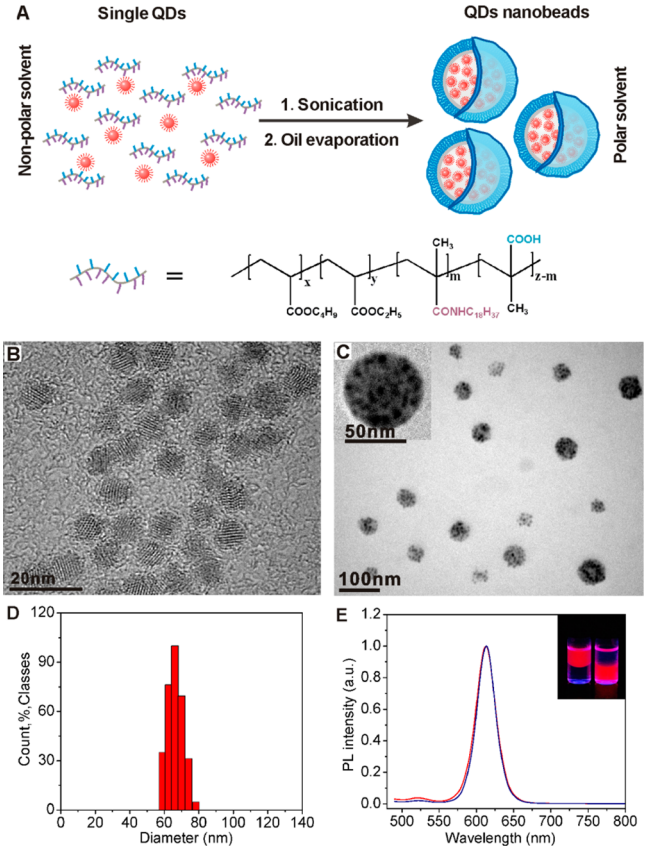

Figure 1. Characterization of the structural and optical properties of the QD nanobeads. (A) Schematic illustration of the QD nanobeads formation mechanism. (B) HRTEM image of the original QDs dissolved in cyclohexane. (C) TEM image of the QD nanobeads dissolved in PBS buffer solution (0.01 M, pH 7.4); the inset shows an individual QD nanobead image at high magnification. (D) Size distribution of the QD nanobeads and (E) identical fluorescence emission spectra of the original QDs dissolved in cyclohexane (blue line) and QD nanobeads dissolved in PBS buffer solution (0.01 M, pH 7.4) (red line).

Figure 1C demonstrates that the QDs were incorporated into the well-isolated ABC-*g*-ODA polymer with a uniform spherical shape of around 60 nm in diameter. The low size dispersity of the QD nanobeads was also confirmed by their polydispersity index (0.162). The surface zeta potentials of the QD nanobeads were −30.9 ± 3.2 mV, and the hydrodynamic size in solution was 68 ± 1.2 nm (Figure 1D). The discrepancy between the two measurements could be attributed to the electrical double layer created by abundant carboxylic acid groups and the swelling of the polymer chains. These two effects increased the colloidal hydrodynamic radius compared to the size observed by TEM, which is recognized as the "dry" size of the particle.[32,33] Spectroscopy measurement (Figure 1E) showed that there was almost no shift in the wavelength of the original QDs compared to that of the QD nanobeads, indicating that the surface ligands of the original QDs were not damaged by the generation of the QD nanobeads. The quantum yield of the QD nanobeads was around 50−70%.

3.2. Characterization of Chemical and Colloidal Stability. The chemical and colloidal stability of QDs is a vital prerequisite for their use in quantitative and sensitive analysis, as the optical properties of QDs are highly sensitive to the environment and fluorescence fluctuation might generate

dx.doi.org/10.1021/am5012782 | ACS Appl. Mater. Interfaces 2014, 6, 6406−6414

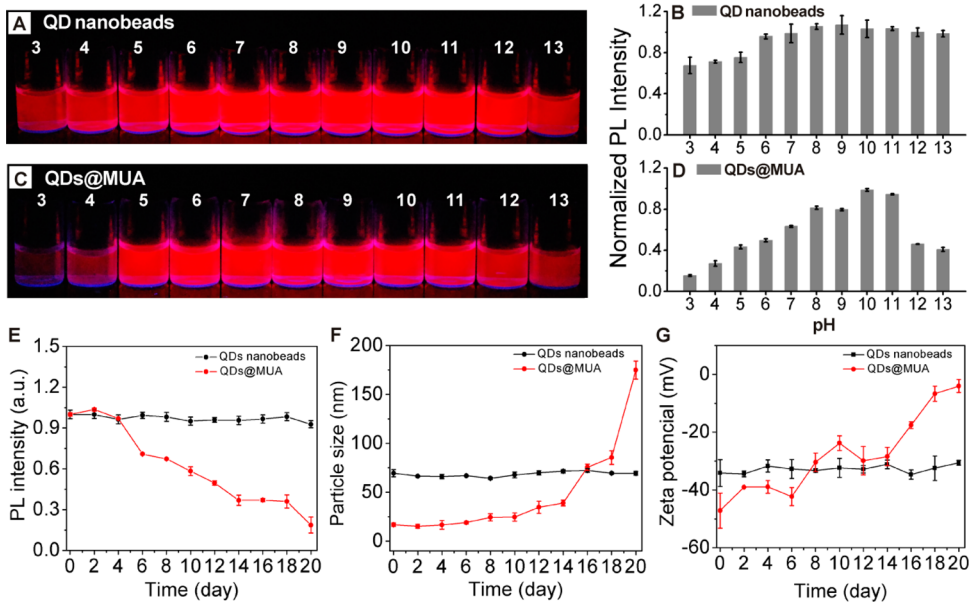

Figure 2. Stability comparison of QD nanobeads and QDs@MUA. Fluorescence images and corresponding intensity profiles of (A, B) QD nanobeads and (C, D) QDs@MUA dispersed in solutions from pH 3 to 13 for 3 days. (E) PL intensity (normalized by PL intensity at pH 7), (F) particle size, and (G) zeta potential of QD nanobeads and QDs@MUA in PBS buffer solution (0.01 M, pH 7.4) with temporal evolution.

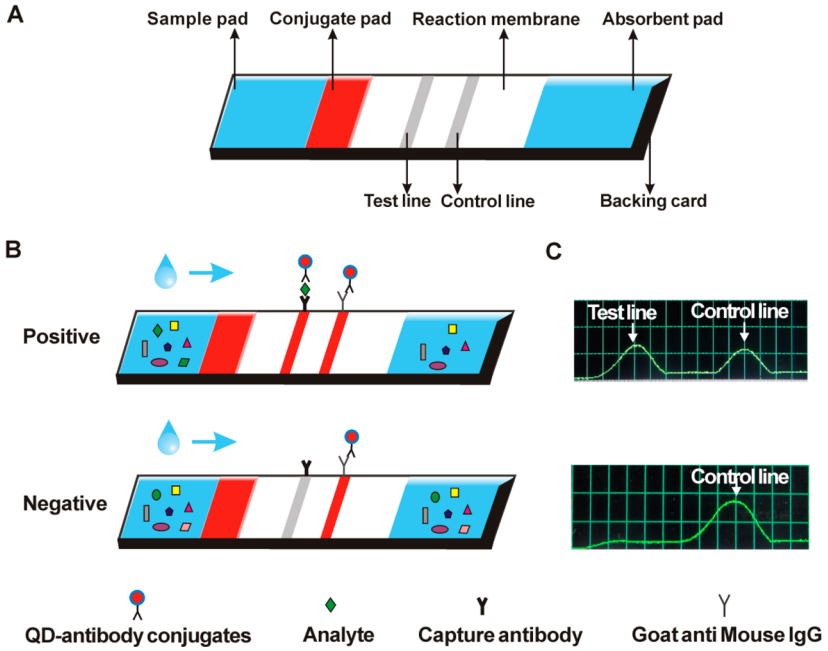

Figure 3. Schematic illustration of ICTS platform detection of cancer protein markers. (A) Typical assembly of the ICTS. (B) Positive tests show two lines, and negative tests show only one line (the control line). (C) The positive and negative tests are displayed by the test strip reader.

inaccurate results.[32] In this experiment, we prepared QDs@MUA and QD nanobeads using the same batch of QDs. As a result, the responding quantum yields of QDs@MUA and QD nanobeads were about 38 and 55%, respectively. To assess the chemical and colloidal stability, the PL intensity of the QDs@MUA and QD nanobeads was first tested after storage in solutions from pH 3 to 13 for 3 days. As can be seen in Figure 2, a clear difference is observed between the QDs@MUA and QD nanobeads (Figure 2). QDs@MUA aggregated and precipitated in both low- and high-pH solutions and maintained relative stability only in a narrow pH range (about 80% in pH 8−11, normalized by fluorescence at pH 7). Compared with that of QDs@MUA, the fluorescence intensity of the QD nanobeads remained constant over the larger pH range of 6−13, and more than 67% of the fluorescence intensity was preserved even at pH 3−5. Even after 20 days, there was more than 40% of the fluorescence intensity at pH 3 (see Supporting Information Figure S2). Both the QDs@MUA and QD nanobeads were stored under physiological conditions and taken for measurements at periodic intervals to further demonstrate their chemical and colloidal stability. Here, PBS buffer solution (0.01 M, pH 7.4) was chosen as the medium. The results from Figure 2E−G suggest that the PL intensity, particle size, and zeta potential of the QD nanobeads are stable

dx.doi.org/10.1021/am5012782 | ACS Appl. Mater. Interfaces 2014, 6, 6406−6414

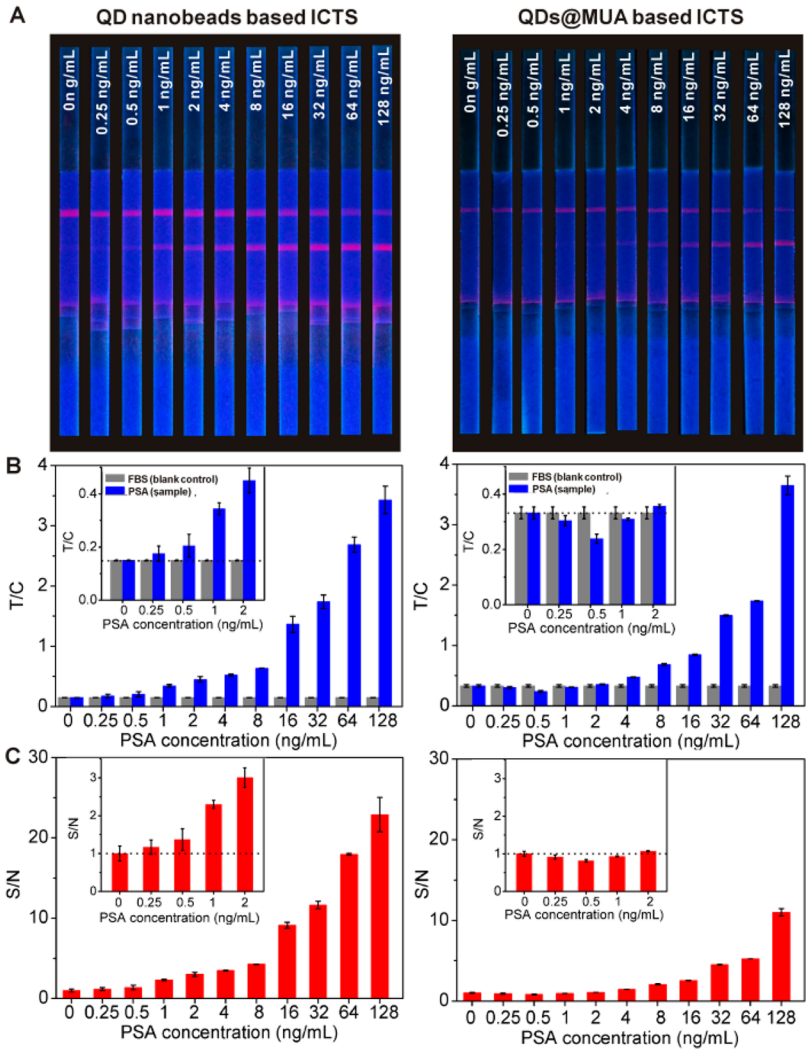

Figure 4. Sensitivity comparison of QD nanobeads- and QDs@MUA-based ICTS platforms. (A) Fluorescence image and corresponding (B) T/C and (C) S/N ratios of QD nanobeads- and QDs@MUA-based ICTS platforms after reaction with 40 μL of samples containing different concentrations of PSA; the inset shows an enlarged view for select PSA concentrations (ranging from 0 to 2 ng/mL).

in PBS buffer during storage for 20 days, indicating their high chemical and colloidal stability. Conversely, QDs@MUA exhibited apparent fluctuations in PL intensity, particle size, and zeta potential during 20 days.

These results provide strong evidence to prove the high chemical and colloidal stability of the QD nanobeads; all of the aforementioned tests are generally used in the literature to discuss the stability of QDs.[34−36] We hypothesize that there are several reasons to account for the outstanding stability of the QD nanobeads: (i) long-chain hydrocarbons (18 carbon) grafted to the ABC triblock copolymer not only interacted with the QDs but also protected QDs from the diffusion of water-soluble compounds through the shell.[37] To demonstrate the importance of ODA, ABC triblock copolymer without any modification was used to encapsulate the QDs. As a result, the products exhibited an irregular shape and poor dispersibility (see Supporting Information Figure S3). (ii) A high-molecular-weight ABC triblock copolymer (100 000 Da) formed a thicker protective layer that provided a nearly complete surface passivation of the QDs.[28,38] (iii) The abundant carboxylic acid groups on the polymer shell surface rendered the QDs water-soluble and provided a negatively charged surface that improved the colloid stability by electrostatic repulsion. In addition, the multishell structure of the QDs synthesized by SILAR was highly stable because the nanocrystals were well-passivated electronically by the radial increase of the respective valence- and conduction-band offsets.[30,31] Therefore, the QD nanobeads that we synthesized can be regarded as an excellent signal-generating reagent for sensitive and quantitative detection in an ICTS platform.

3.3. ICTS Platform Design. As schematically illustrated in Figure 3, a test strip usually needs several functionalities that are typically realized with five components: a sample pad, a conjugate pad, a reaction membrane, an absorbent pad, and a backing card (Figure 3A). A sample was dropped on the sample pad, and it migrated through the test strip by capillary action. The principle of the ICTS test is based on sandwich assays. Generally, if an analyte is in a sample, then it will interact with the QD−antibody conjugates and then will be captured on the test zone to generate a positive result (Figure 3B). If no analyte is present, then only QD−antibody conjugates will be bound to the control zone, returning a negative result (Figure 3B). The results from the reaction membrane were interpreted as the presence or absence of signal in the test zone, which was read either by the naked eye with hand-held ultraviolet lamp excitation or with a strip reader to read the fluorescence

dx.doi.org/10.1021/am5012782 | ACS Appl. Mater. Interfaces 2014, 6, 6406−6414

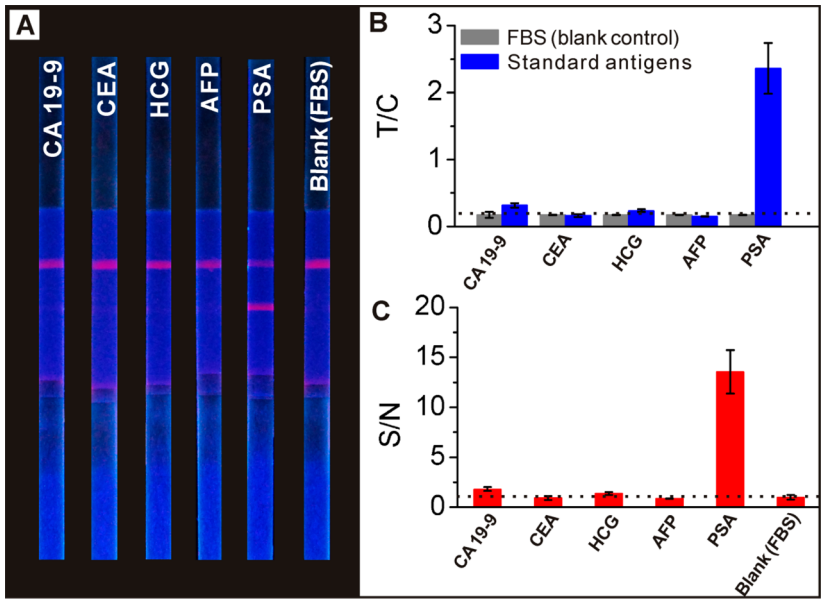

Figure 5. Characterization of the specificity of the QD nanobeads-based ICTS platform. (A) Fluorescence image and corresponding (B) T/C and (C) S/N ratios of the QD nanobeads-based ICTS platform after reaction with 40 μL of samples containing different standard antigens (CA19-9, CEA, HCG, AFP, and PSA at 50 ng/mL) or FBS (blank control).

intensity. Herein, the fluorescence intensity ratio between the test zone and the control zone (T/C) was used to determine the amount of analyte in the sample. The signal-to-noise ratio (S/N) was defined as the fluorescence peak area ratio between the target and the blank control samples. Detection results using the strips were analyzed three times by the test strip reader, and the average values were plotted as a function of analyte's concentration.[24]

3.4. Effect of the Signal-Generating Reagent. The particle size was optimized to maximize the T/C and S/N ratios. A small fraction of large particles were obtained by low-speed centrifugation after their preparation to study the influence of particle size on the signal that they produce. There were three different signal-generating reagents with different particle sizes, from 15 to 130 nm, including QDs@MUA (~15 nm), QD nanobeads (~68 nm), and QD nanobeads (~130 nm). Fluorescent measurements were performed under the same conditions (10 ng/mL PSA, 40 μL). T/C and S/N ratios were tested to determine the most efficient particle size. As seen in Figure S3, the T/C ratio of QDs@MUA was obviously lower than that of the QD nanobeads. Although the highest T/C ratio was measured by the QD nanobeads with a size of 150 nm, the highest nonspecific binding was measured at the same time (Figure S3B). Therefore, the maximal S/N ratio was obtained by the QD nanobeads with a size of 68 nm (Figure S3C).

We attributed the optimal S/N ratio to the signal-generating reagent that we elaborated: (i) the outstanding chemical stability and colloid stability of the QD nanobeads effectively resisted the potential fluorescent decrease or particle aggregation during the preparation of the ICTS, for example, QDs specimens often exhibit deterioration in the course of bioconjugation[37] and (ii) proper particle size is important for the signal response.[39,40] To further investigate the effect of the particle size on the fluorescence response, the fluorescence intensity fluctuation on the test zone of the three different signal-generating reagents was monitored within 30 min under the same targeting molecule conditions. As seen in Figure S5, the smaller particle generated a fluorescence response in a rather short amount of time, although it produced the weakest fluorescence intensity. The larger particle generated a stronger fluorescence intensity and required a longer time. In view of the S/N ratio, the fluorescence intensity, and the reaction time, QD nanobeads with a 68 nm diameter were identified as the optimized signal-generating reagent in our study; thus, they hold promise for improving the sensitivity of the ICTS.

3.5. Characterization of the QD Nanobeads-Based ICTS Platform. For the practical application of point-of-care diagnostics, the operation should be quick and simple, as opposed to conventional techniques that rely on large and complex instruments and skilled personnel. In our study, the assay was done simply by adding a small amount of sample (40 μL) on the sample pad, and the results were easily interpreted by the naked eye or using the strip reader. On the basis of the optimized conditions, the properties of the ICTS were comprehensively characterized in different formats.

The effective reaction time, ranging from 5 to 30 min, was investigated by using 40 μL of samples containing 10 ng/mL PSA; FBS without PSA was used as a blank control (see Supporting Information). The T/C and S/N ratios were tested to determine the effective reaction time. As displayed in Figure S4, the detectable T/C ratio emerged 5 min after samples were applied. Both the T/C or S/N ratios reached a constant value at 15 min, which revealed that 15 min was enough time for an effective reaction. Thus, the T/C and S/N ratios for quantitative analysis were measured 15 min after sample addition in all of the succeeding studies.

The detection sensitivity of the ICTS was characterized by analyzing standard PSA samples at a concentration gradient of 0−128 ng/mL diluted in FBS; FBS without PSA was used as a blank control. Qualitatively, Figure 4 reveals that the brightness of the test zone (Figure 4A), the T/C ratio (Figure 4C), and the S/N ratio (Figure 4D) were increased with the increasing concentrations of PSA. Compared with the ICTS using QDs@MUA as the signal-generating reagent, our QD nanobeads-based ICTS afforded increased sensitivity owing to the robust

dx.doi.org/10.1021/am5012782 | ACS Appl. Mater. Interfaces 2014, 6, 6406−6414

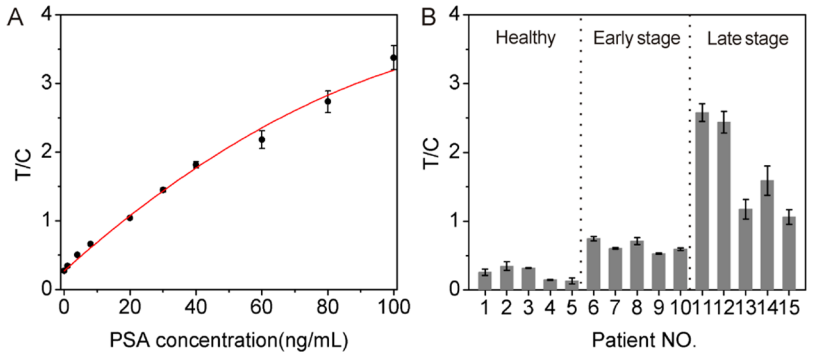

Figure 6. Quantitative detection in clinical samples. (A) Calibration curve of the quantitative detection by the QD nanobeads-based ICTS platform. (B) Results of the clinical serum specimens analyzed with the QD nanobeads-based ICTS platform.

signal-generating reagent. With the QD nanobeads-based ICTS, the detection limit was 0.33 ng/mL, which was defined as being three times the blank control sample's (FBS) standard deviation (S/N = 3). The standard error was based on three duplicate measurements of the analytes. The detection sensitivity afforded an enhancement by up to ~12-fold (~3.87 ng/mL) compared with that of the QDs@MUA-based ICTS (Figure 4). In the event that the concentration of the analyte is low, an ICTS with low sensitivity are not viable because the intensity of the fluorescent band in the test zone is too weak to be detected. These results indicate that with the use of the QD nanobeads as the signal-generating reagent the sensitivity of the ICTS can be improved effectively.

To determine the specificity of the ICTS, five groups of analytes were used. Herein, the strip with PSA added was used as the test group; the strips with carbohydrate antigen 19-9 (CA19-9), carchinoembryonic antigen (CEA), human chorionic gonadotropin (HCG), and alpha-fetoprotein (AFP) added were used as the negative control group; the strip with FBS added was used as the blank control group. If nonspecific binding exists, then the protein markers from the negative control group would be recognized by the QD−PSA conjugates and captured on the test zone. Consequently, the signal response of the test zone would be obviously higher than that from the blank control group. Figure 5A shows an image of all of the groups, in which a clear distinction can be observed between the test and control groups. For the test group, an obvious fluorescent band of the test and control zones was observed (Figure 5A). The T/C (Figure 5B) and S/N (Figure 5C) ratios were remarkably higher than those in the blank control group. At the same time, there was no crosstalk or interference with the negative control group that was observed by naked eye (Figure 5A) or the test strip reader (Figure 5B,C). These features provide strong evidence of the high specificity of the ICTS.

The QD nanobeads-based ICTS could be readily applied for the detection of other cancer biomarkers by changing the antibody conjugated to the QD nanobeads and immobilizing them on the test zone. To assess the potential applications in the detection of various cancer biomarkers, AFP and HCG monoclonal antibodies were conjugated to the QD nanobeads, respectively. Abnormal AFP and HCG serum concentrations are closely associated with liver cancer and gestational trophoblastic diseases, respectively. As expected, high specificity was successfully detected (see Supporting Information Figure S5). These results indicate that the ICTS platform might be versatile for detecting different cancer biomarkers.

3.6. Quantitative Detection in Clinical Samples. The ability to use the QD nanobeads-based ICTS for quantitative analysis was corroborated by their calibration curve and their use for clinical sample analysis (Figure 6). The calibration curve for PSA quantification was obtained by recording the T/C ratio of different PSA concentrations using the test strip reader under optimized conditions.[24] Error bars represent the standard deviation of the mean over the three sets of duplicate measurements of the analytes. As indicated in Figure 6A, the data could be fit to a polynomial with $r^2 = 0.9936$ ($y = 0.27114 + 0.04294x - (1.371 \times 10^{-4})x^2$). The detection limit of 0.33 ng/mL was well below the commonly accepted threshold level in clinical diagnosis for prostate cancer.[2] Typically, the PSA serum concentration at the early stages of prostate cancer is from 4 to 10 ng/mL, whereas the normal level is from 0.5 to 2 ng/mL. Late-stage prostate cancer is characterized by values higher than 10 ng/mL. Furthermore, to evaluate the potential clinical application of the QD nanobeads-based ICTS platform, clinical serum samples from PSA-positive patients were analyzed, and serum samples from healthy patients without PSA were used as the negative control. Results obtained using a commercial PSA kit were defined as being true positive and true negative. As showed in Figure 6B, the assay detected the presence of PSA in all PSA-positive patient samples. Meanwhile, the T/C ratio was at the baseline level for the control samples. Therefore, these results indicate that the QD nanobeads-based ICTS platform demonstrates promise for the quantitative detection of PSA markers in clinical applications.

4. CONCLUSIONS

A well-performing ICTS platform was designed by combining it with fabricated QD nanobeads for the quantitative detection of cancer protein biomarkers. The QD nanobeads possessed a proper particle size as well as outstanding chemical and colloidal stability compared with that of QDs@MUA, making them a unique and effective signal-generating reagent. The integration enabled the ICTS platform to sensitively and specifically determine the concentration of PSA using only 40 μL samples in 15 min. Under the optimized conditions, the detection limit was enhanced by about ~12-fold compared with that of the QDs@MUA-based ICTS. The measurements in patient serum samples demonstrated the possible clinical utility of this approach. Moreover, it provided one-step detection without extensive purification steps and an easy readout for nonprofessional operators. In view of its advantages, the QD nanobeads-based ICTS platform may be a nascent sensing

technology that opens up new opportunities for the early detection of cancer or other diseases at the site of patient care.

■ ASSOCIATED CONTENT

Supporting Information

Reaction route and ^{1}H NMR spectra of ABC-*g*-ODA; fluorescence images and corresponding intensity profiles of QD nanobeads in solutions of different pH after 20 days; TEM image of the QDs coated with ABC triblock copolymer; DLS, T/C, and S/N of signal reagents; fluorescence intensity of the test zone generated by three different signal reagents; effect of immunoreaction time using the ICTS platform; and characterization of the versatility of the ICTS platform. This material is available free of charge via the Internet at http://pubs.acs.org.

■ AUTHOR INFORMATION

Corresponding Authors

*(L.X.) E-mail: xuanlx@hotmail.com.

*(J.C.) E-mail: jinchang@tju.edu.cn. Tel./Fax: +86-022-27401821.

Notes

The authors declare no competing financial interest.

■ ACKNOWLEDGMENTS

The authors gratefully acknowledge the National High Technology Program of China (863 Program) (2012AA022603), the Natural Science Foundation of China (51373117 and 81171372), the Key Project of the Tianjin Applied Basic Research Program (13JCZDJC33200), and the Doctoral Base Foundation of the Educational Ministry of China (20120032110027).

■ REFERENCES

(1) Kulasingam, V.; Diamandis, E. P. Strategies for Discovering Novel Cancer Biomarkers through Utilization of Emerging Technologies. *Nat. Clin. Pract. Oncol.* **2008**, *5*, 588−599.

(2) Etzioni, R.; Urban, N.; Ramsey, S.; McIntosh, M.; Schwartz, S.; Reid, B.; Radich, J.; Anderson, G.; Hartwell, L. The Case for Early Detection. *Nat. Rev. Cancer* **2003**, *3*, 243−252.

(3) Pantel, K.; Brakenhoff, R. H.; Brandt, B. Detection, Clinical Relevance and Specific Biological Properties of Disseminating Tumour Cells. *Nat. Rev. Cancer* **2008**, *8*, 329−340.

(4) Hall, E. A. H. In *Handbook of Biosensors and Biochips*; Marks, R. S., Cullen, D. C., Karube, I., Lowe, C. R., Weetall, H. H., Eds.; Wiley: Chichester, England, 2007; Chapter 72, pp 1111−1129.

(5) Holland, C. A.; Kiechle, F. L. Point-of-Care Molecular Diagnostic Systems-Past, Present and Future. *Curr. Opin. Microbiol.* **2005**, *8*, 504−509.

(6) Lai, G.; Yan, F.; Ju, H. Dual Signal Amplification of Glucose Oxidase-Functionalized Nanocomposites as a Trace Label for Ultrasensitive Simultaneous Multiplexed Electrochemical Detection of Tumor Markers. *Anal. Chem.* **2009**, *81*, 9730−9736.

(7) Qian, J.; Gao, X. Triblock Copolymer-Encapsulated Nanoparticles with Outstanding Colloidal Stability for siRNA Delivery. *ACS Appl. Mater. Interfaces* **2013**, *5*, 2845−2852.

(8) Zhou, Y.; Pan, F. G.; Li, Y. S.; Zhang, Y. Y.; Zhang, J. H.; Lu, S. Y.; Ren, H. L.; Liu, Z. S. Colloidal Gold Probe-Based Immunochromatographic Assay for the Rapid Detection of Brevetoxins in Fishery Product Samples. *Biosens. Bioelectron.* **2009**, *24*, 2744−2747.

(9) Mao, X.; Xu, H.; Zeng, Q.; Zeng, L.; Liu, G. Molecular Beacon-Functionalized Gold Nanoparticles as Probes in Dry-Reagent Strip Biosensor for DNA Analysis. *Chem. Commun.* **2009**, 3065−3067.

(10) Suárez-Pantaleón, C.; Wichers, J.; Abad-Somovilla, A.; van Amerongen, A.; Abad-Fuentes, A. Development of an Immunochromatographic Assay Based on Carbon Nanoparticles for the Determination of the Phytoregulator Forchlorfenuron. *Biosens. Bioelectron.* **2012**, *42*, 170−176.

(11) Danks, C.; Barker, I. On-Site Detection of Plant Pathogens Using Lateral-Flow Devices. *EPPO Bull.* **2000**, *30*, 421−426.

(12) Karakus, C.; Salih, B. A. Comparison of the Lateral Flow Immunoassays (LFIA) for the Diagnosis of *Helicobacter pylori* Infection. *J. Immunol. Methods* **2013**, *396*, 8−14.

(13) Corstjens, P. L.; Zuiderwijk, M.; Nilsson, M.; Feindt, H.; Sam Niedbala, R.; Tanke, H. J. Lateral-Flow and Up-Converting Phosphor Reporters To Detect Single-Stranded Nucleic Acids in a Sandwich-Hybridization Assay. *Anal. Biochem.* **2003**, *312*, 191−200.

(14) Corstjens, P. L.; van Lieshout, L.; Zuiderwijk, M.; Kornelis, D.; Tanke, H. J.; Deelder, A. M.; van Dam, G. J. Up-Converting Phosphor Technology-Based Lateral Flow Assay for Detection of Schistosoma Circulating Anodic Antigen in Serum. *J. Clin. Microbiol.* **2008**, *46*, 171−176.

(15) Xu, Q.; Xu, H.; Gu, H.; Li, J.; Wang, Y.; Wei, M. Development of Lateral Flow Immunoassay System Based on Superparamagnetic Nanobeads as Labels for Rapid Quantitative Detection of Cardiac Troponin I. *Mater. Sci. Eng., C* **2009**, *29*, 702−707.

(16) Wang, D. B.; Tian, B.; Zhang, Z. P.; Deng, J. Y.; Cui, Z. Q.; Yang, R. F.; Wang, X. Y.; Wei, H. P.; Zhang, X. E. Rapid Detection of *Bacillus anthracis* Spores Using a Super-Paramagnetic Lateral-Flow Immunological Detectionsystem. *Biosens. Bioelectron.* **2013**, *42*, 661−667.

(17) Khreich, N.; Lamourette, P.; Boutal, H.; Devilliers, K.; Créminon, C.; Volland, H. Detection of *Staphylococcus* Enterotoxin B Using Fluorescent Immunoliposomes as Label for Immunochromatographic Testing. *Anal. Biochem.* **2008**, *377*, 182−188.

(18) Khreich, N.; Lamourette, P.; Lagoutte, B.; Ronco, C.; Franck, X.; Créminon, C.; Volland, H. A Fluorescent Immunochromatographic Test Using Immunoliposomes for Detecting Microcystins and Nodularins. *Anal. Bioanal. Chem.* **2010**, *397*, 1733−1742.

(19) Rosi, N. L.; Mirkin, C. A. Nanostructures in Biodiagnostics. *Chem. Rev.* **2005**, *105*, 1547−1562.

(20) Guo, W. Synthesis of Zn-Cu-In-S/ZnS Core/Shell Quantum Dots with Inhibited Blue-Shift Photoluminescence and Applications for Tumor Targeted Bioimaging. *Theranostics* **2013**, *3*, 99−108.

(21) Liu, H. Y.; Gao, X. Engineering Monovalent Quantum Dot-Antibody Bioconjugates with a Hybrid Gel System. *Bioconjugate Chem.* **2011**, *22*, 510−517.

(22) Guo, W.; Chen, N.; Dong, C.; Tu, Y.; Chang, J.; Zhang, B. One-Pot Synthesis of Hydrophilic ZnCuInS/ZnS Quantum Dots for in Vivo Imaging. *RSC Adv.* **2013**, *3*, 9470−9475.

(23) Li, Z.; Wang, Y.; Wang, J.; Tang, Z.; Pounds, J. G.; Lin, Y. Rapid and Sensitive Detection of Protein Biomarker Using a Portable Fluorescence Biosensor Based on Quantum Dots and a Lateral Flow Test Strip. *Anal. Chem.* **2010**, *82*, 7008−7014.

(24) Yang, Q.; Gong, X.; Song, T.; Yang, J.; Zhu, S.; Li, Y.; Cui, Y.; Li, Y.; Zhang, B.; Chang, J. Quantum Dot-Based Immunochromatography Test Strip for Rapid, Quantitative and Sensitive Detection of Alpha Fetoprotein. *Biosens. Bioelectron.* **2011**, *30*, 145−150.

(25) Chan, W. C.; Nie, S. Quantum Dot Bioconjugates for Ultrasensitive Nonisotopic Detection. *Science* **1998**, *281*, 2016−2018.

(26) Zhang, T.; Stilwell, J. L.; Gerion, D.; Ding, L.; Elboudwarej, O.; Cooke, P. A.; Gray, J. W.; Alivisatos, A. P.; Chen, F. F. Cellular Effect of High Doses of Silica-Coated Quantum Dot Profiled with High Throughput Gene Expression Analysis and High Content Cellomics Measurements. *Nano Lett.* **2006**, *6*, 800−808.

(27) Dubertret, B.; Skourides, P.; Norris, D. J.; Noireaux, V.; Brivanlou, A. H.; Libchaber, A. In Vivo Imaging of Quantum Dots Encapsulated in Phospholipid Micelles. *Science* **2002**, *298*, 1759−1762.

(28) Gao, X.; Cui, Y.; Levenson, R. M.; Chung, L. W.; Nie, S. In Vivo Cancer Targeting and Imaging with Semiconductor Quantum Dots. *Nat. Biotechnol.* **2004**, *22*, 969−976.

(29) Anderson, R. E.; Chan, W. C. Systematic Investigation of Preparing Biocompatible, Single, and Small ZnS-Capped CdSe Quantum Dots with Amphiphilic Polymers. *ACS Nano* **2008**, *2*, 1341−1352.

(30) Li, J. J.; Wang, Y. A.; Guo, W.; Keay, J. C.; Mishima, T. D.; Johnson, M. B.; Peng, X. Large-Scale Synthesis of Nearly Monodisperse CdSe/CdS Core/Shell Nanocrystals Using Air-Stable Reagents via Successive Ion Layer Adsorption and Reaction. *J. Am. Chem. Soc.* **2003**, *125*, 12567−12575.
(31) Xie, R.; Kolb, U.; Li, J.; Basché, T.; Mews, A. Synthesis and Characterization of Highly Luminescent CdSe-Core $CdS/Zn_{0.5}Cd_{0.5}S$/ZnS Multishell Nanocrystals. *J. Am. Chem. Soc.* **2005**, *127*, 7480−7488.
(32) Yang, J.; Dave, S. R.; Gao, X. Quantum Dot Nanobarcodes: Epitaxial Assembly of Nanoparticle-Polymer Complexes in Homogeneous Solution. *J. Am. Chem. Soc.* **2008**, *130*, 5286−5292.
(33) Cui, Y.; Gong, X.; Zhu, S.; Li, Y.; Su, W.; Yang, Q.; Chang, J. An Effective Modified Method to Prepare Highly Luminescent, Highly Stable Water-Soluble Quantum Dots and Its Preliminary Application in Immunoassay. *J. Mater. Chem.* **2012**, *22*, 462−469.
(34) Giovanelli, E.; Muro, E.; Sitbon, G.; Hanafi, M.; Pons, T.; Dubertret, B.; Lequeux, N. Highly Enhanced Affinity of Multidentate versus Bidentate Zwitterionic Ligands for Long-Term Quantum Dot Bioimaging. *Langmuir* **2012**, *28*, 15177−15184.
(35) Smith, A. M.; Duan, H.; Rhyner, M. N.; Ruan, G.; Nie, S. A Systematic Examination of Surface Coatings on the Optical and Chemical Properties of Semiconductor Quantum Dots. *Phys. Chem. Chem. Phys.* **2006**, *8*, 3895−3903.
(36) Liu, J.; Song, T.; Yang, Q.; Tan, J.; Huang, D.; Chang, J. Highly Stable Quantum Dots with Silica-Poly(EGDMA-co-MAA) Synergistic Protection and the Preliminary Application in Immunoassay. *J. Mater. Chem. B* **2013**, *1*, 1156−1163.
(37) Hu, X.; Gao, X. Silica-Polymer Dual Layer-Encapsulated Quantum Dots with Remarkable Stability. *ACS Nano* **2010**, *4*, 6080−6086.
(38) Liu, Z.; Davis, C.; Cai, W.; He, L.; Chen, X.; Dai, H. Circulation and Long-Term Fate of Functionalized, Biocompatible Single-Walled Carbon Nanotubes in Mice Probed by Raman Spectroscopy. *Proc. Natl. Acad. Sci. U.S.A.* **2008**, *105*, 1410−1415.
(39) Laitinen, M.; Vuento, M. Affinity Immunosensor for Milk Progesterone: Identification of Critical Parameters. *Biosens. Bioelectron.* **1996**, *11*, 1207−1214.
(40) Posthuma-Trumpie, G. A.; Korf, J.; van Amerongen, A. Lateral Flow (Immuno) Assay: Its Strengths, Weaknesses, Opportunities and Threats. A Literature Survey. *Anal. Bioanal. Chem.* **2009**, *393*, 569−582.